Journal of Power Sources 185 (2008) 534–541

Contents lists available at ScienceDirect

Journal of Power Sources

journal homepage: www.elsevier.com/locate/jpowsour

Synthesis and electrochemistry of cubic rocksalt Li–Ni–Ti–O compounds in the phase diagram of $LiNiO_2$–$LiTiO_2$–$Li[Li_{1/3}Ti_{2/3}]O_2$

Lianqi Zhang[a,*], Hideyuki Noguchi[a], Decheng Li[a], Takahisa Muta[a], Xiaoqing Wang[a], Masaki Yoshio[a], Izumi Taniguchi[b]

[a] Department of Applied Chemistry, Saga University, Saga 840-8052, Japan
[b] Department of Chemical Engineering, Tokyo Institute of Technology, 12-1, Ookayama-2, Meguro-ku, Tokyo 152-8552, Japan

ARTICLE INFO

Article history:
Received 8 August 2007
Received in revised form 17 March 2008
Accepted 12 June 2008
Available online 1 July 2008

Keywords:
Lithium ion batteries
Phase diagram of $LiNiO_2$–$LiTiO_2$–$Li[Li_{1/3}Ti_{2/3}]O_2$
Cubic rocksalt Li–Ni–Ti–O
Spray-drying

ABSTRACT

On the basis of extreme similarity between the triangle phase diagrams of $LiNiO_2$–$LiTiO_2$–$Li[Li_{1/3}Ti_{2/3}]O_2$ and $LiNiO_2$–$LiMnO_2$–$Li[Li_{1/3}Mn_{2/3}]O_2$, new Li–Ni–Ti–O series with a nominal composition of $Li_{1+z/3}Ni_{1/2-z/2}Ti_{1/2+z/6}O_2$ ($0 \le z \le 0.5$) was designed and attempted to prepare via a spray-drying method. XRD identified that new Li–Ni–Ti–O compounds had cubic rocksalt structure, in which Li, Ni and Ti were evenly distributed on the octahedral sites in cubic closely packed lattice of oxygen ions. They can be considered as the solid solution between cubic $LiNi_{1/2}Ti_{1/2}O_2$ and $Li[Li_{1/3}Ti_{2/3}]O_2$ (high temperature form). Charge–discharge tests showed that Li–Ni–Ti–O compounds with appropriate compositions could display a considerable capacity (more than 80 mAh g^{-1} for $0.2 \le z \le 0.27$) at room temperature in the voltage range of 4.5–2.5 V and good electrochemical properties within respect to capacity (more than 150 mAh g^{-1} for $0 \le z \le 0.27$), cycleability and rate capability at an elevated temperature of 50 °C. These suggest that the disordered cubic structure in some cases may function as a good host structure for intercalation/deintercalation of Li^+. A preliminary electrochemical comparison between $Li_{1+z/3}Ni_{1/2-z/2}Ti_{1/2+z/6}O_2$ ($0 \le z \le 0.5$) and $Li_{6/5}Ni_{2/5}Ti_{2/5}O_2$ indicated that charge–discharge mechanism based on Ni redox at the voltage of >3.0 V behaved somewhat differently, that is, Ni could be reduced to +2 in $Li_{1+z/3}Ni_{1/2-z/2}Ti_{1/2+z/6}O_2$ while +3 in $Li_{6/5}Ni_{2/5}Ti_{2/5}O_2$. Reduction of Ti^{4+} at a plateau of around 2.3 V could be clearly detected in $Li_{1+z/3}Ni_{1/2-z/2}Ti_{1/2+z/6}O_2$ with $0.27 \le z \le 0.5$ at 50 °C after a deep charge associated with charge compensation from oxygen ion during initial cycle.

1. Introduction

The search for a new cathode material for Li-ion battery is still ongoing task. Layered Li–Ni–Mn–O compounds recently received renewed attention [1–17]. They are $Li[Ni_{1/2-z/2}Li_{z/3}Mn_{1/2+z/6}]O_2$ ($0 \le z \le 1$) [1–13], $Li[Ni_zLi_{1/3-z/3}Mn_{2/3-2z/3}]O_2$ ($0 \le z \le 1$) [14], $Li[Ni_{1-z}Mn_z]O_2$ ($0 \le z \le 0.5$) [15] and $Li_{1+z}[Ni_{1/2}Mn_{1/2}]_{1-z}O_2$ ($0 \le z \le 0.2$) [6,16,17] series. Alternatively, they can be rewritten in a composite notation as $z/2LiNiO_2 \cdot z/2LiMnO_2 \cdot (1-z)Li[Li_{1/3}Mn_{2/3}]O_2$ ($0 \le z \le 1$), $zLiNiO_2 \cdot (1-z)Li[Li_{1/3}Mn_{2/3}]O_2$ ($0 \le z \le 1$), $(1-z)LiNiO_2 \cdot zLiMnO_2$ ($0 \le z \le 0.5$) and $(1-z)/2LiNiO_2 \cdot (1-5z)/2LiMnO_2 \cdot 3zLi[Li_{1/3}Mn_{2/3}]O_2$ ($0 \le z \le 0.2$), respectively. As a result, all the compounds can be described by a triangle phase diagram of $LiNiO_2$–$LiMnO_2$–$Li[Li_{1/3}Mn_{2/3}]O_2$, as indicated in Fig. 1. In fact, this phase diagram has been adopted to pursue new layered Li–Ni–Mn–O compounds in our early study [14], but true understanding of the phase diagram was not given at that time. Along with the revisiting of $LiNi_{1/2}Mn_{1/2}O_2$, the nature of transitional Ni and Mn ions was re-recognized in the as-prepared material and during electrochemical cycling [9–13]. Ni and Mn in $LiNi_{1/2}Mn_{1/2}O_2$ existed as +2 and +4 oxidation states, respectively, and Ni acted as the electrochemically active species from +2 to +4 during cycling in the voltage range of >2.5 V, while Mn^{4+} was electrochemically inert and functioned as a stable framework. Therefore, $LiNi_{1/2}Mn_{1/2}O_2$ should be considered as a new compound instead of a simple solid solution between layered $LiNiO_2$ and $LiMnO_2$ [13], taking into account its valence difference of transitional metal ions from those in $LiNiO_2$ and $LiMnO_2$. Accordingly, all the reported layered rocksalt Li–Ni–Mn–O compounds prepared by a high temperature solid state reaction during the past decades [1–18], without considering the super structure due to ordering of metal ions in the layers containing transitional metal ions [5,6,19–21], may be simply considered as the solid solutions between the compounds of layered $LiNiO_2$, $Li[Li_{1/3}Mn_{2/3}]O_2$ and $LiNi_{1/2}Mn_{1/2}O_2$.

* Corresponding author. Present address: Tianjin Institute of Power Sources, No. 18, Lingzhuangzi road, Nankai-qu, Tianjin 300381, China. Tel.: +86 22 23959613; fax: +86 22 23383783.
E-mail addresses: zhanglianqi@gmail.com, zhanglianqi@mailcity.com (L. Zhang).

0378-7753/$ – see front matter © 2008 Elsevier B.V. All rights reserved.
doi:10.1016/j.jpowsour.2008.06.054

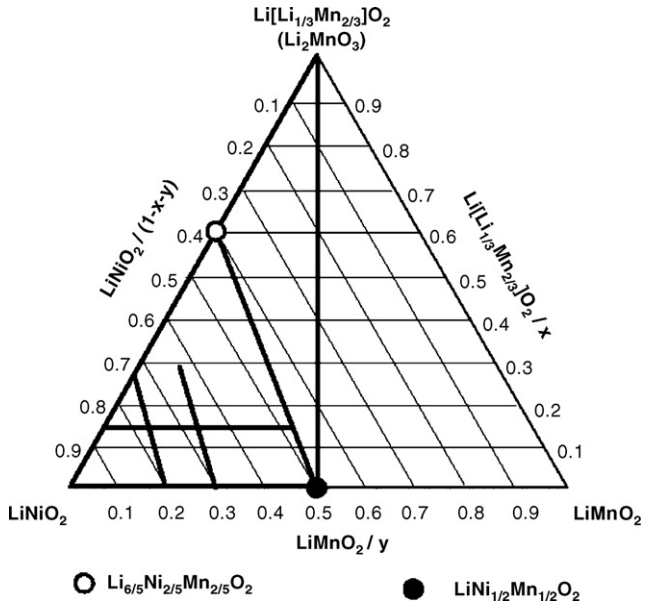

Fig. 1. Composition triangle in the system of $LiNiO_2$–$LiMnO_2$–$Li[Li_{1/3}Mn_{2/3}]O_2$. The bold lines represent the compositions which have been reported as a single phase via a high temperature solid state reaction in the references [1–18].

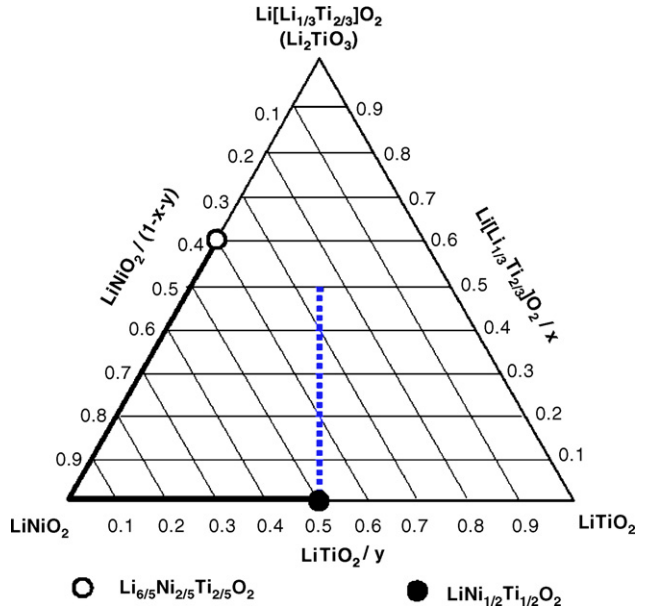

Fig. 2. Composition triangle in the system of $LiNiO_2$–$LiTiO_2$–$Li[Li_{1/3}Ti_{2/3}]O_2$. The bold lines represent the compositions which have been reported as a single phase via a high temperature solid state reaction in the references [25–32]. The dashed line was prepared in this work.

The pure phase region can roughly be on and on the left of the line between $LiNi_{1/2}Mn_{1/2}O_2$ and $Li[Li_{1/3}Mn_{2/3}]O_2$. In addition, complex charge–discharge processes were also found in some Li–Ni–Mn–O compounds [4,5,21–23].

Among Li–Ti–O compounds, $Li[Li_{1/3}Ti_{2/3}]O_2$ (low temperature form) can has a similar layered rocksalt structure to $Li[Li_{1/3}Mn_{2/3}]O_2$ [24] and Ti more tends to exist as +4. Therefore, an analog of $LiNiO_2$–$LiMnO_2$–$Li[Li_{1/3}Mn_{2/3}]O_2$ triangle phase diagram, $LiNiO_2$–$LiTiO_2$–$Li[Li_{1/3}Ti_{2/3}]O_2$ system, possibly exists. In comparison with Mn, Ti is lighter and has the stronger bonding capability with O. Of more importance, Ti^{4+} usually has a reduction potential at a potential less than 2.5 V vs. Li, which benefits clarifying electrochemical reaction mechanism. Indeed, two series of Li–Ni–Ti–O compounds marked as bold lines in Fig. 2 were already reported [25–32] and Ni in compounds could be +3, mixture of +2 and +3, or +2 with Ti^{4+}, as occurring in Li–Ni–Mn–O system. $LiNi_{1/2}Ti_{1/2}O_2$ similar to $LiNi_{1/2}Mn_{1/2}O_2$ should be also judged as a new compound, at least because of its valence difference from $LiNiO_2$ and $LiTiO_2$. Therefore, it can be also speculated that the similar pure phase region in the phase diagram of $LiNiO_2$–$LiTiO_2$–$Li[Li_{1/3}Ti_{2/3}]O_2$ possibly can be obtained as observed in Li–Ni–Mn–O system. Nevertheless, structure in the reported Li–Ni–Ti–O compounds gradually became disordered with increasing Ti content [26,31,32]. In the cases of $LiNi_{1/2}Ti_{1/2}O_2$ and $Li_{6/5}Ni_{2/5}Ti_{2/5}O_2$, structure almost was a cubic one. Despite the structural difference between layered $LiNiO_2$ and disordered $LiNi_{1/2}Ti_{1/2}O_2$ (or $Li_{6/5}Ni_{2/5}Ti_{2/5}O_2$), structural mergence between $LiNiO_2$, $LiNi_{1/2}Ti_{1/2}O_2$, and $Li_{6/5}Ni_{2/5}Ti_{2/5}O_2$ still happens to form a series of pure rocksalt-structured compounds. This is possibly because they all belong to rocksalt structure. Therefore, the reported Li–Ni–Ti–O compounds may be simply considered as solid solutions based on the rocksalt structure (solid solution is defined in the light of rocksalt structure and layered ordering in rocksalt structure is neglected. In fact, cation disorder in $Li[Ni_{1-z}Mn_z]O_2$ also gradually increases and reaches a value of about 10% for Ni occupancy in Li layers in $LiNi_{1/2}Mn_{1/2}O_2$. The difference in $LiNi_{1/2}Ti_{1/2}O_2$ is that the value reaches about 50%). More interestingly, $Li_{6/5}Ni_{2/5}Ti_{2/5}O_2$ despite the disordered structure still could display impressive electrochemical properties [26]. We found that a much excess charge capacity over the theoretical one based on Ni^{4+}/Ni^{3+} redox species and an almost theoretical discharge capacity in the initial cycle were observed with good subsequent cycling at an elevated temperature.

In this work, to demonstrate that pure phase compounds in the phase diagram of $LiNiO_2$–$LiTiO_2$–$Li[Li_{1/3}Ti_{2/3}]O_2$ can be similarly obtained as in the phase diagram of $LiNiO_2$–$LiMnO_2$–$Li[Li_{1/3}Mn_{2/3}]O_2$, new Li–Ni–Ti–O compounds with the nominal composition of $Li_{1+z/3}Ni_{1/2-z/2}Ti_{1/2+z/6}O_2$ ($0 \le z \le 0.5$) (partial connecting line between $LiNi_{1/2}Ti_{1/2}O_2$ and $Li[Li_{1/3}Ti_{2/3}]O_2$) was selected and tentatively prepared by a spray-drying method. They have a same substitution mechanism as $Li[Ni_{1/2-z/2}Li_{z/3}Mn_{1/2+z/6}]O_2$ ($0 \le z \le 1$). The new series presumably will have disordered structure because Ti content is larger than that in $LiNi_{1/2}Ti_{1/2}O_2$ or $Li_{6/5}Ni_{2/5}Ti_{2/5}O_2$. However, they have higher theoretical capacity based on Ni redox species than $Li_{6/5}Ni_{2/5}Ti_{2/5}O_2$. Their charge–discharge performances at room and elevated temperatures were explored. A preliminary comparison to $Li_{6/5}Ni_{2/5}Ti_{2/5}O_2$ in electrochemical properties was given to further clarify charge–discharge mechanism in disordered Li–Ni–Ti–O compounds.

2. Experimental

Materials were prepared by a spray-drying method [26]. Briefly, stoichiometric $LiOH{\cdot}H_2O$, Ni $(CH_3COO)_2{\cdot}4H_2O$ and titanium coating solution (the acidic solution of $[NH_4]_2[Ti(C_2O_4)_3]$) (TKC-305, Tayca Co.) were dissolved in water with the aid of citric acid. The transparent solution was fed into a spray-drying instrument (pulvis mini-spray GB22, Yamato, Japan) to produce a homogenous precursor. The precursor was initially decomposed at 400 °C in air and then ground after cooling. The decomposed mixture was finally calcined at 750 °C for 15 h in air and O_2 for $Li_{1+z/3}Ni_{1/2-z/2}Ti_{1/2+z/6}O_2$ ($0 \le z \le 0.5$) and $Li_{6/5}Ni_{2/5}Ti_{2/5}O_2$, respectively. The samples were ground again after cooling and then kept in a desiccator with blue silica-gel. The color of $Li_{1+z/3}Ni_{1/2-z/2}Ti_{1/2+z/6}O_2$ ($0 \le z \le 0.5$) was bright green while $Li_{6/5}Ni_{2/5}Ti_{2/5}O_2$ presented a color of 'dark brown'.

The crystallographic properties of samples were characterized using a Rigaku diffractometer (RINT 1000) with Cu Kα radiation. The scan electron microscope (SEM) images were obtained by JEOL JSM-5200 electron microscope. The specific surface area for samples was analyzed by the Brunauer, Emmett, and Teller (BET) method using Micromeritics Gemini2375, where N_2 gas absorption was employed. Samples were heated to 200 °C for 20 min to remove the absorbed moisture prior to measurement. Fourier transform infrared (FTIR) spectra were collected by a KBr method using FT/IR-4100 (JASCO) spectroscopy. The content of lithium, nickel and titanium in partial materials was analyzed using an inductively coupled plasmas spectrometer (ICP, SPS 7800, Seiko Instruments, Japan).

The charge and discharge characteristics of Li–Ni–Ti–O cathodes were examined in CR2032 coin-type half-cell (Li/Li–Ni–Ti–O). Cells were composed of a cathode and a lithium metal anode (Cyprus Foote Mineral Co.) separated by a porous polypropylene film (Celgard 3401). The cathode consisted of 20 mg active material and 12 mg conductive binder [8 mg polytetrafluoroethylene (PTFE) and 4 mg acetylene black]. It was pressed on a stainless steel mesh at 800 kg cm^{-2} and then dried in vacuum at 150 °C for 6 h. The electrolyte solution was a 1:2 mixture of ethylene carbonate (EC) and dimethylcarbonate (DMC) containing 1 M $LiPF_6$. All cells were assembled in an argon-filled dry box. Cells were galvanostatically cycled under different conditions.

3. Results and discussion

XRD patterns of $Li_{1+z/3}Ni_{1/2-z/2}Ti_{1/2+z/6}O_2$ ($0 \le z \le 0.5$) are shown in Fig. 3 (left panel). All reflections can be indexed to a cubic rocksalt structure of alpha-$LiFeO_2$ with space group of F_{m3m} (No. 225) [33]. Thus, Li and transitional metals (Ni and Ti) should evenly occupy the octahedral sites in cubic closely packed oxygen lattice. With increasing z value, total XRD presented a gradual left shift, which was reflected as an almost linear increase in lattice parameter as shown in Fig. 4. This suggests the formation of solid solution, which can be further supported well by the continuous change in recorded FTIR spectra of $Li_{1+z/3}Ni_{1/2-z/2}Ti_{1/2+z/6}O_2$ as indicated in the right panel of Fig. 3. In the wavelength range of 400–800 cm^{-1}, mainly two peaks were observed in FTIR spectra for these samples. The peaks can be associated with vibrations of Li–O and M–O bonds (M = Ni and Ti) [32] and gradually shifted to a higher value with increasing z value.

$Li_{1+z/3}Ni_{1/2-z/2}Ti_{1/2+z/6}O_2$ ($0 \le z \le 0.5$) exhibited a color of 'bright green' in sharp contrast to 'dark brown' of $Li_{6/5}Ni_{2/5}Ti_{2/5}O_2$. The

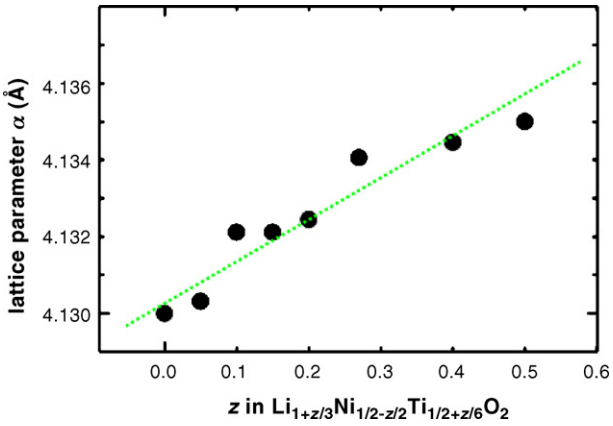

Fig. 4. Change of lattice constant as a function of z in $Li_{1+z/3}Ni_{1/2-z/2}Ti_{1/2+z/6}O_2$ ($0 \le z \le 0.5$). The dashed line is the fitting plot.

compounds of $Ni(OH)_2$ and NiO(OH) containing Ni^{2+} and Ni^{3+} have green and black colors, respectively. Therefore, it is evident that Ni valence should be +2 and +3 in $Li_{1+z/3}Ni_{1/2-z/2}Ti_{1/2+z/6}O_2$ and $Li_{6/5}Ni_{2/5}Ti_{2/5}O_2$, respectively, considering that Ti^{4+} is colorless. Careful comparison of the two samples, $LiNi_{1/2}Ti_{1/2}O_2$ ($z = 0$) and $Li_{6/5}Ni_{2/5}Ti_{2/5}O_2$, can give more information. Two compounds have the same ratio of Ni vs. Ti and thus $Li_{6/5}Ni_{2/5}Ti_{2/5}O_2$ can be obtained only by adding excess Li in the synthesis of $LiNi_{1/2}Ti_{1/2}O_2$. The chemical composition analysis of the resultant samples, $LiNi_{1/2}Ti_{1/2}O_2$ and $Li_{6/5}Ni_{2/5}Ti_{2/5}O_2$, indeed indicated little deviation in the atomic ratio of three metal elements, Li, Ni and Ti, from the aimed values. A weak 0 0 3 reflection in a layered structure at the 2θ of about 18.7° can be still observed in $Li_{6/5}Ni_{2/5}Ti_{2/5}O_2$ while it basically disappeared in $LiNi_{1/2}Ti_{1/2}O_2$, as shown in Fig. 5. Furthermore, all reflection positions were also different, thus causing quite different lattice parameters in a cubic cell as indicated in figure (Strictly, XRD pattern of $Li_{6/5}Ni_{2/5}Ti_{2/5}O_2$ should be indexed to a hexagonal system due to the appearance of 0 0 3 reflection). Additionally, electrochemical properties were also significantly different as shown later. Thus, it can be believed that excess Li are really incorporated into $LiNi_{1/2}Ti_{1/2}O_2$ structure to form $Li_{6/5}Ni_{2/5}Ti_{2/5}O_2$, accompanying transformation of Ni^{2+} to Ni^{3+} and thus color change of materials. $Li_{1+z/3}Ni_{1/2-z/2}Ti_{1/2+z/6}O_2$ ($0 \le z \le 0.5$) can be strictly considered as the solid solution between cubic rocksalt $LiNi_{1/2}Ti_{1/2}O_2$ and $Li[Li_{1/3}Ti_{2/3}]O_2$ (high temperature form [34]) in the light of composition, valence and structure.

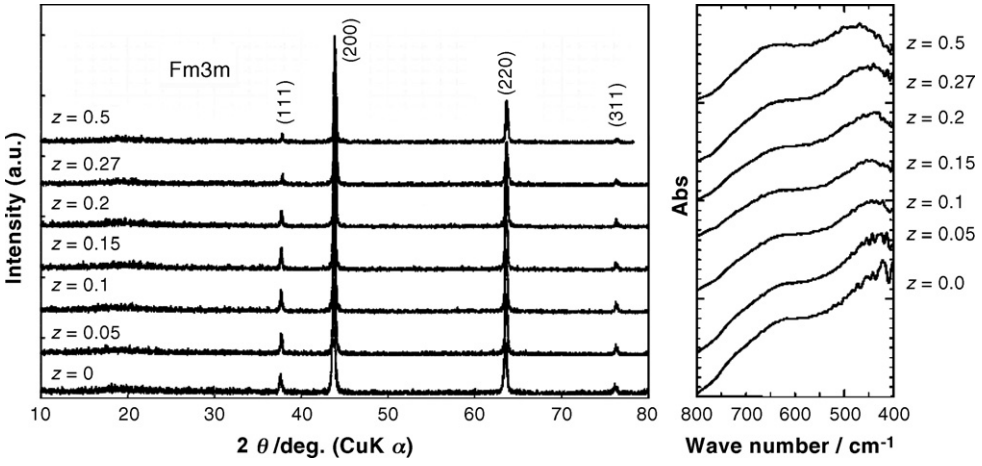

Fig. 3. XRD patterns (left panel) and FTIR spectra (right panel) of $Li_{1+z/3}Ni_{1/2-z/2}Ti_{1/2+z/6}O_2$ ($0 \le z \le 0.5$).

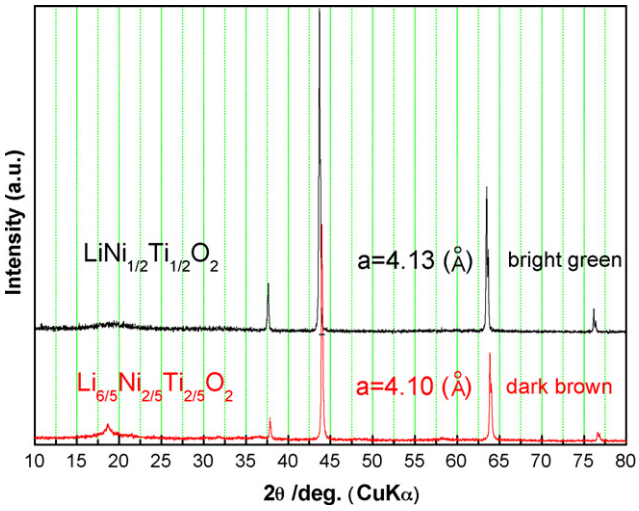

Fig. 5. Comparison of $LiNi_{1/2}Ti_{1/2}O_2$ ($z=0$) and $Li_{6/5}Ni_{2/5}Ti_{2/5}O_2$ in XRD patterns.

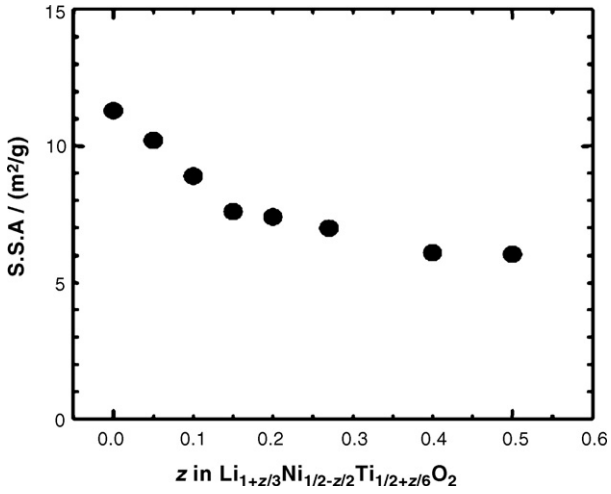

Fig. 7. Change of BET surface area as a function of z in $Li_{1+z/3}Ni_{1/2-z/2}Ti_{1/2+z/6}O_2$ ($0 \le z \le 0.5$).

If we extrapolate the plot of lattice constant as a function of z in $Li_{1+z/3}Ni_{1/2-z/2}Ti_{1/2+z/6}O_2$ as indicated in Fig. 4, the lattice constant for cubic $Li[Li_{1/3}Ti_{2/3}]O_2$ can be around 4.141 Å, which indeed agrees well with the reported 4.140 Å [35]. The linear change in lattice parameter can be reasonably explained as below. In the solid solution, there is a substitution equation of $3Ni^{2+} = 2Li^+ + Ti^{4+}$. The ionic radii of Li^+, Ni^{2+} and Ti^{4+} are 0.76, 0.69 and 0.60 Å, respectively [36]; therefore, the average ionic radius of $[2Li^+ + Ti^{4+}]$ (0.707 Å) is larger than that of Ni^{2+}. The larger mean ionic radius can cause expansion of lattice with increasing z. Similarly, from $LiNi_{1/2}Ti_{1/2}O_2$ to $Li_{6/5}Ni_{2/5}Ti_{2/5}O_2$ there is such a substitution as $5Ni^{2+} + Ti^4 = 2Li^+ + 4Ni^{3+}$. The average ionic radius of $[2Li^+ + 4Ni^{3+}]$ (0.627 Å) is smaller than that of $[5Ni^{2+} + Ti^{4+}]$ (0.675 Å), thus causing the shrinkage of lattice of $Li_{6/5}Ni_{2/5}Ti_{2/5}O_2$.

Fig. 6 shows the SEM images of the two typical samples with $z = 0.0$ and 0.2 in $Li_{1+z/3}Ni_{1/2-z/2}Ti_{1/2+z/6}O_2$ ($0 \le z \le 0.5$). Severe agglomeration of primary into larger particles could be observed, which made the observation of primary particle difficult in our experiments. Roughly, the samples seemed to have nanosized primary particles with a size less than 100 nm. This is supported by the calculation of crystallite size using the Scherer equation below from X-ray reflection in 200 plane:

$$\delta = \frac{0.9\lambda}{B \cos \theta} \quad (1)$$

where δ is crystallite size; λ, average of Cu Kα1 and Kα2; B, the full width at half maximum of 200 peak in radian; θ, the diffraction angle. The average crystallite size of power for the sample with $z = 0$ is about 40 nm. Nanosized powders resulted in a considerably large surface area as indicated in Fig. 7. The surface area displayed monotonous decrease with increasing z in $Li_{1+z/3}Ni_{1/2-z/2}Ti_{1/2+z/6}O_2$ ($0 \le z \le 0.5$).

Charge–discharge tests for several typical samples at a constant current density of 0.2 mA cm^{-2} (20 mA g^{-1}) in the voltage range of 4.5–2.5 V at a room temperature (about 25 °C) are shown in Fig. 8. The sample with $z = 0.27$ delivered the largest charge–discharge capacities of about 160 and 85 mAh g^{-1} with smooth charge–discharge curves, as summarized in Fig. 10. However, when they were charge–discharged at an elevated temperature of about 50 °C as shown in Fig. 9, charge capacity increased from about 200 to 300 mAh g^{-1} with increasing z value from 0 to 0.5 and the samples with $0 \le z \le 0.27$ could deliver a discharge capacity of around 150 mAh g^{-1}. It is surprising in a disorder structure, because our conventional wisdom is that cations mixing in layered compounds like $LiNiO_2$ will produce vitally detrimental effects on charge–discharge performances and the compounds with disorder rocksalt structure such as alpha-$LiFeO_2$ will be electrochemically inactive. The conventional wisdom was indeed confirmed in most of recent reports in $LiNi_{1-z}Ti_zO_2$ compounds [25,28–30,32]. However, a recent report on nanosized disordered $LiNi_{1/2}Ti_{1/2}O_2$ prepared via a sol–gel like route at a low temperature of 600 °C showed considerable electrochemical activity [31], which is contrary to $LiNi_{1/2}Ti_{1/2}O_2$ prepared via a high temperature solid state reaction showing little electrochemical reaction [32]. The sim-

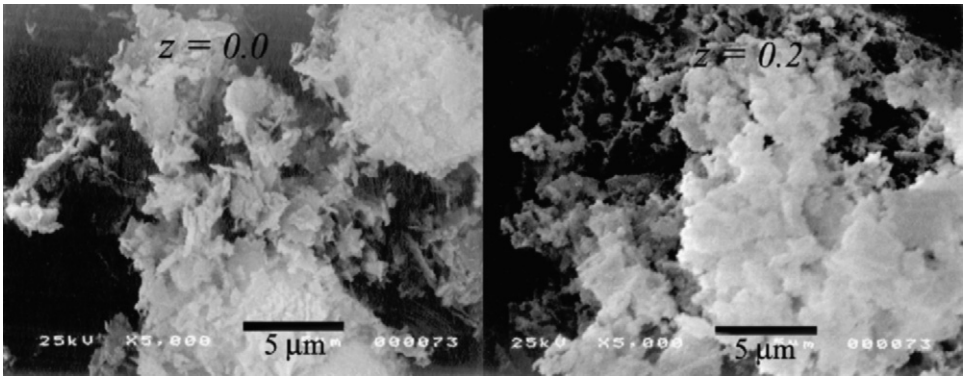

Fig. 6. SEM images of $Li_{1+z/3}Ni_{1/2-z/2}Ti_{1/2+z/6}O_2$ with $z = 0$ and 0.2.

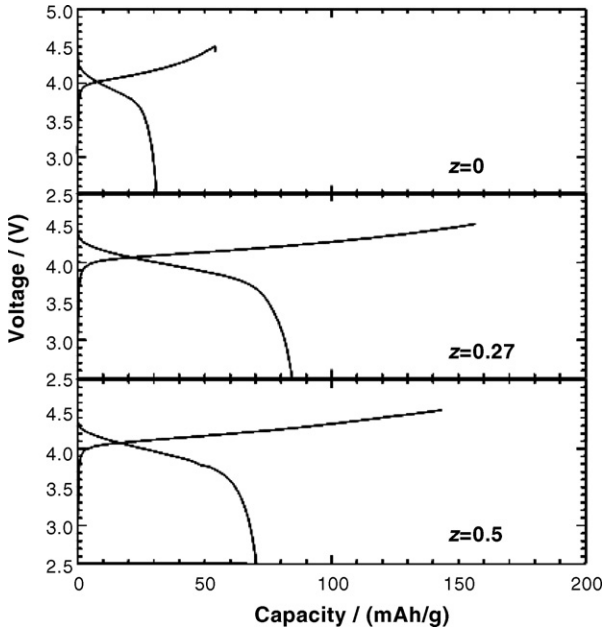

Fig. 8. Initial charge–discharge curves of several typical samples in $Li_{1+z/3}Ni_{1/2-z/2}Ti_{1/2+z/6}O_2$ ($0 \le z \le 0.5$) cycled in the voltage range of 4.5–2.5 V at a constant current density of 0.2 mA cm^{-2} (20 mA g^{-1}) at a room temperature (about 25 °C).

ilar phenomenon was also reported in nanosized Li–Fe–Ti–O with disordered structure [35]. The crystallite size possibly with several tens of nanometers for $Li_{1+z/3}Ni_{1/2-z/2}Ti_{1/2+z/6}O_2$ ($0 \le z \le 0.5$) was also obtained as mentioned above, which we believe should play a key role for good electrochemical activity for these samples.

All the observed capacities at room temperature lay in the range of the calculated one based on oxidization of Ni^{2+} to Ni^{4+}; nevertheless, the charge capacity of the samples with $z > 0.27$ exceeded the calculated one at 50 °C as shown in Fig. 10, accompanying

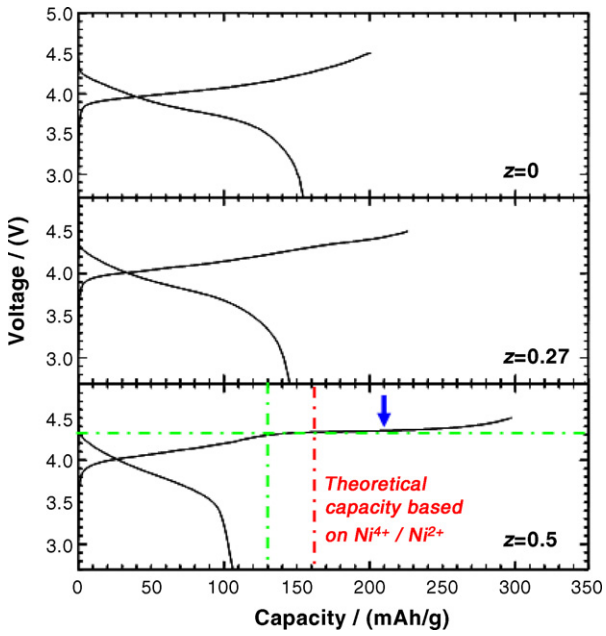

Fig. 9. Initial charge–discharge curves of several typical samples in $Li_{1+z/3}Ni_{1/2-z/2}Ti_{1/2+z/6}O_2$ ($0 \le z \le 0.5$) cycled in the voltage range of 4.5–2.7 V at a constant current density of 0.2 mA cm^{-2} (20 mA g^{-1}) at an elevated temperature (around 50 °C).

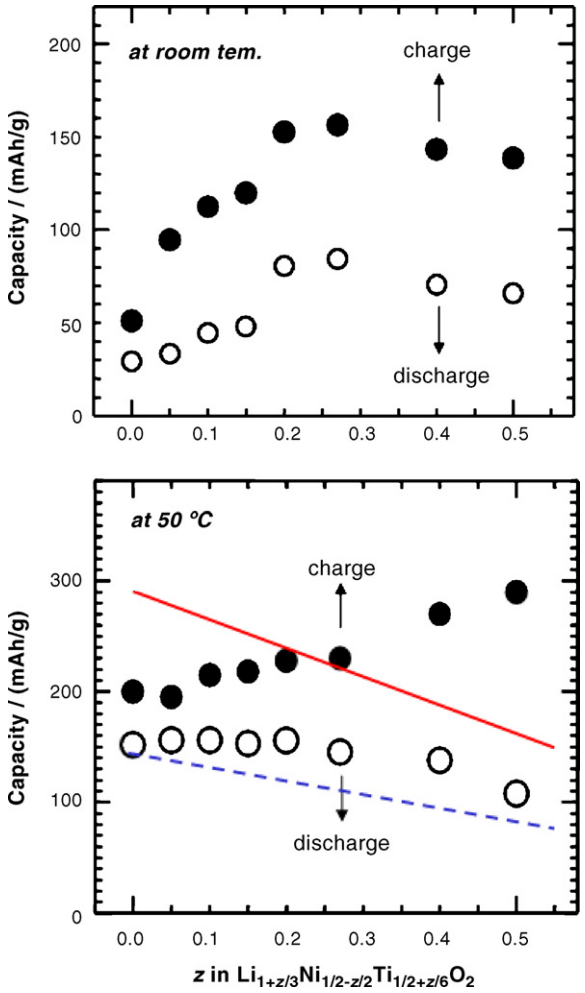

Fig. 10. The summary of initial charge–discharge capacities observed in Figs. 8 and 9. The solid (red) and dashed (blue) lines represent the calculated capacities based on Ni^{4+}/Ni^{2+} and Ni^{4+}/Ni^{3+} redox species in $Li_{1+z/3}Ni_{1/2-z/2}Ti_{1/2+z/6}O_2$ ($0 \le z \le 0.5$), respectively. (For interpretation of the references to color in this figure legend, the reader is referred to the web version of the article.)

the appearance of a charge voltage at around 4.4 V as pointed by the arrow in Fig. 9. This phenomenon was also observed in $Li[Ni_{1/2-z/2}Li_{z/3}Mn_{1/2+z/6}]O_2$ ($0 \le z \le 1$) and $Li_{4/3-z/3}Ni_zTi_{2/3-2z/3}O_2$ ($0 \le z \le 0.4$) series, which was ascribed to simultaneous loss of O and Li [4,5,22,23,26]. In $Li[Ni_{1/2-z/2}Li_{z/3}Mn_{1/2+z/6}]O_2$ ($0 \le z \le 1$), partial Mn^{4+} was reduced to Mn^{3+} at the voltage of >2.5 V after charge compensation from oxygen ions during initial charge process, thus causing a large discharge capacity. Two typical samples with $z = 0.5$ and 0.27 were also discharged to a lower voltage of 1.5 V to examine if Ti^{4+} can be reduced after charged to different capacities at 50 °C, as indicated in Fig. 11. Indeed, an evident discharge plateau at around 2.3 V was clearly observed for $z = 0.5$ after a deep charge (c and d in top panel of Fig. 11). This discharge plateau without doubt can be deduced as the reduction of Ti^{4+}, because the discharge capacity could exceed the calculated one based on the redox species of Ni^{4+}/Ni^{2+}. However, the discharge capacity at the voltage of >2.5 V, which should be contributed from Ni redox species, at best lay in the middle site between the calculated capacities based on Ni^{4+}/Ni^{3+} and Ni^{4+}/Ni^{2+} for the sample with $z = 0.5$. This seems to suggest that Ni cannot be completely reduced to +2 at a voltage of 2.5 V. However, careful observation of charge process for $z = 0.5$ indicated that the initial charge plateau at around 4.4 V associated with charge compensation from oxygen ion occurred at about 130 mAh g^{-1},

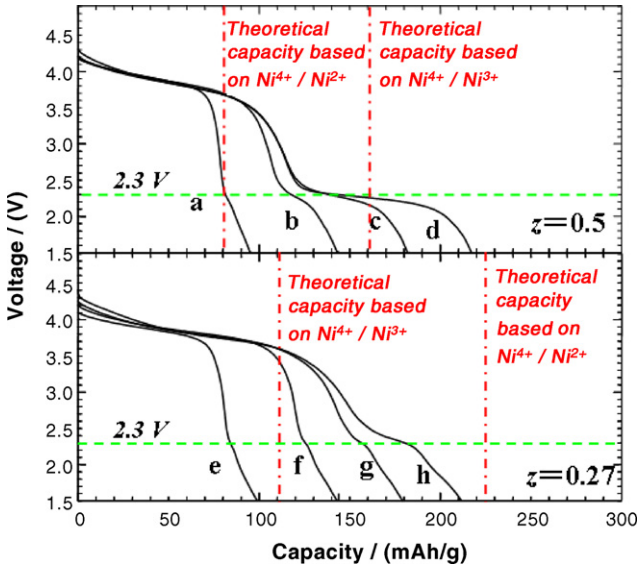

Fig. 11. Initial discharge curves of the samples with $z = 0.5$ and 0.27 discharged to 1.5 V after the cells were charged to different depths: (a) 110 mAh g^{-1}; (b) 150 mAh g^{-1}; (c) 190 mAh g^{-1}; (d) 250 mAh g^{-1}; (e) 125 mAh g^{-1}; (f) 170 mAh g^{-1}; (g) 210 mAh g^{-1}; (h) 255 mAh g^{-1}.

which was much earlier than the calculated 161.9 mAh g^{-1} based on the redox species of Ni^{4+}/Ni^{2+}, as indicated in Fig. 9. This suggests that Ni possibly cannot be completely oxidized to +4 during charge process under the conditions used here, which thus causes a lower discharge capacity at the voltage of >2.5 V. Furthermore, all discharge capacities of $Li_{1+z/3}Ni_{1/2-z/2}Ti_{1/2+z/6}O_2$ ($0 \le z \le 0.5$) at the voltage of >2.7 V at 50 °C lay between the calculated capacities based on Ni^{4+}/Ni^{3+} and Ni^{4+}/Ni^{2+}, as indicated in Fig. 10. Therefore, it can be believed that redox species of Ni^{4+}/Ni^{3+} and Ni^{3+}/Ni^{2+} should be responsible for the discharge capacity at the voltage of >2.7 V. In addition, the length of discharge plateau at 2.3 V for the sample with $z = 0.5$ was closely correlated with that of the initial charge plateau at 4.4 V. This can be well supported by the plot in Fig. 12, where the discharge capacity below 2.5 V had a linear relationship with excess charge capacity over 130 mAh g^{-1}. The observation of the discharge plateau at a low voltage of 2.3 V associated with Ti^{4+} reduction as well as its linear correlation with the initial charge plateau can in turn support the proposed electrochemical redox

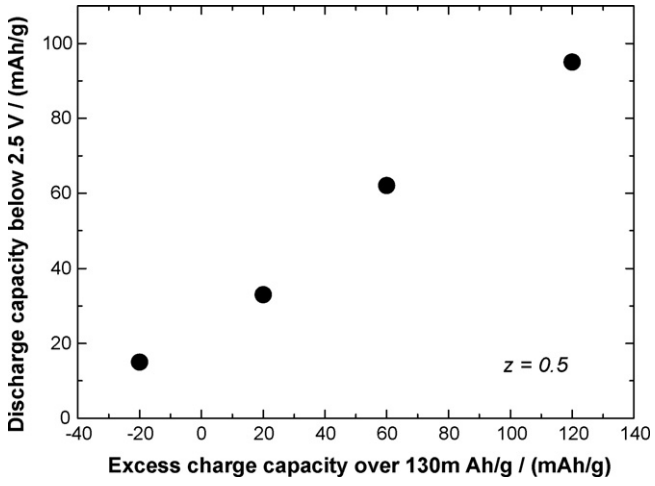

Fig. 12. Plot of discharge capacity below 2.5 V (in Fig. 11) against excess charge capacity over 130 mAh g^{-1} in the sample with $z = 0.5$.

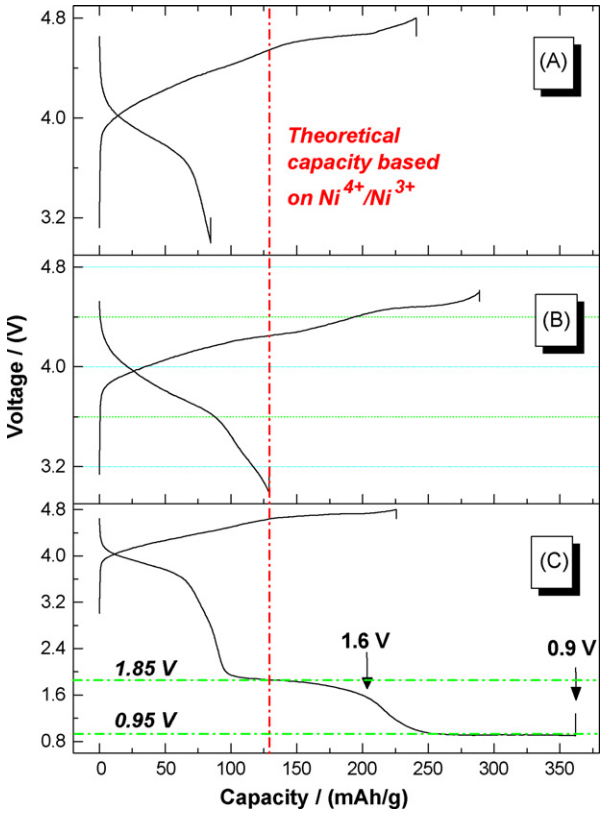

Fig. 13. Initial charge–discharge curves of $Li_{6/5}Ni_{2/5}Ti_{2/5}O_2$ at a constant current density of 0.2 mA cm^{-2} (20 mA g^{-1}) under different conditions: (A) in the voltage range of 4.8–3.0 V at room temperature (about 25 °C); (B) in the voltage range of 4.6–3.0 V at 60 °C; (C) in the voltage range of 4.8–0.9 V at room temperature.

mechanism that the charge plateau is associated with the simultaneous expulsion of O and Li, instead of electrolyte decomposition and even oxidation of O^{2-} to O^{-}. For the sample with $z = 0.27$, the discharge plateau at around 2.3 V could be also clearly detected only after the deep charge to 255 mAh g^{-1} (about 30 mAh g^{-1} excess capacity over the calculated one based on the redox species of Ni^{4+}/Ni^{2+}).

Nevertheless, $Li_{6/5}Ni_{2/5}Ti_{2/5}O_2$ with almost disordered structure appeared to present some discrepancies to $Li_{1+z/3}Ni_{1/2-z/2}Ti_{1/2+z/6}O_2$ ($0 \le z \le 0.5$) in electrochemistry, according to our previously reported data [26]. Fig. 13 shows initial charge–discharge curves of $Li_{6/5}Ni_{2/5}Ti_{2/5}O_2$ under different conditions. An excess charge capacity over the calculated capacity of oxidation of transitional metals to +4 was similarly observed when cells were charged to 4.8 V or cycled at an elevated temperature, but the charge plateau was not as apparent as in the samples with $z = 0.4$ and 0.5. Moreover, a calculated discharge capacity based on Ni^{4+}/Ni^{3+} was almost observed in the voltage range of 4.6–3.0 V at around 60 °C, suggesting that Ni was not reduced to +2 at the voltage of >3.0 V. When discharged to a lower voltage of 0.9 V at room temperature, $Li_{6/5}Ni_{2/5}Ti_{2/5}O_2$ displayed additional two discharge plateaus at around 1.85 and 0.95 V, respectively. It seems that the discharge plateau at around 1.85 V may be assigned to reduction of Ti^{4+} according to the phenomenon observed in $Li_{1+z/3}Ni_{1/2-z/2}Ti_{1/2+z/6}O_2$ ($0 \le z \le 0.5$); however, additional insertion of Li into tetrahedral site of $LiNiO_2$ to form Li_2NiO_2 occurred at around 1.9 V [37], accompanying the reduction of Ni^{3+} to Ni^{2+}. After the plateau at 1.85 V, actually all octahedral sites in cubic closely packed lattice of oxygen should be occupied as indicated in Fig. 13, and thus the additional insertion of Li into

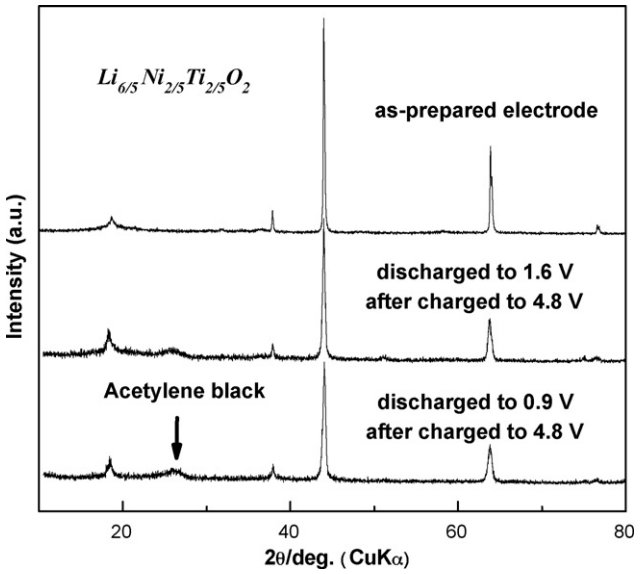

Fig. 14. Ex situ XRD patterns of the electrode as-prepared and cycled to different low potentials in $Li_{6/5}Ni_{2/5}Ti_{2/5}O_2$.

tetrahedral sites possibly happens at 0.95 V in $Li_{6/5}Ni_{2/5}Ti_{2/5}O_2$. $LiNi_{1/2}Mn_{1/2}O_2$ was reported to have additional insertion of one Li at around 1.0 V [11,38], but it was associated with the reduction of Mn^{4+}. Therefore, it is somewhat difficult here to make clear the electrochemical reaction mechanism at the low voltage of <2.5 V in $Li_{6/5}Ni_{2/5}Ti_{2/5}O_2$. Further careful comparison and investigations such as in situ measurements of X-ray absorption are needed to reach a clear conclusion. Although ex situ XRD may not be reliable enough at such a low voltage as 0.9 V, it was still finished as supplementary data. The ex situ XRD patterns for the electrodes discharged to 1.6 and 0.9 V as pointed by arrows in the C panel of Fig. 13 are shown in Fig. 14. Results showed that the structure was maintained well in the electrodes discharged to the low potentials.

$Li_{1+z/3}Ni_{1/2-z/2}Ti_{1/2+z/6}O_2$ ($0 \le z \le 0.5$) could also exhibit surprisingly good rate discharge performance at 50 °C. The discharge capability of the samples with $z = 0$ and 0.2 at different rates in the voltage range of 4.5–2.5 V are illuminated in Fig. 15. The sample with $z = 0$ at 0.1C (20 mA g^{-1} and 0.2 mA cm^{-2}, C is defined as 200 mAh g^{-1}) could generate a discharge capacity more than 150 mAh g^{-1} and discharge capacity only reduced to about 116 mAh g^{-1} after increasing discharge rate to 2C (400 mA g^{-1} and 4 mA cm^{-2}). The sample with $z = 0.2$ similarly exhibited a discharge capacity more than 160 mAh g^{-1} at 0.1C and maintained around 78% capacity (about 125 mAh g^{-1}) at 2C. This suggests that discharge rate exerts little effect on discharge capacity at 50 °C despite disorder structure.

The cycleability for several typical samples under the conditions executed in Figs. 8 and 9 is shown in Fig. 16. The samples indicated good cycling performances at room temperature and stable cycleability after some capacity loss during initial several cycles at 50 °C. An optimized composition may be $0.2 \le z \le 0.27$. The samples with these compositions could deliver a considerable capacities more than 80 mAh g^{-1} at room temperature and more than 150 mAh g^{-1} at 50 °C in the voltage range of 4.5–2.5 V. Good cycleability and excellent rate capability at the elevated temperature could be also observed. These suggest that the disordered cubic structure in some electrode materials sometimes may work well for extraction and insertion of Li^+. Presumably, this can be associated with nanosize effect of powder and 'pillar effect' of the framework consisting of Ti^{4+}.

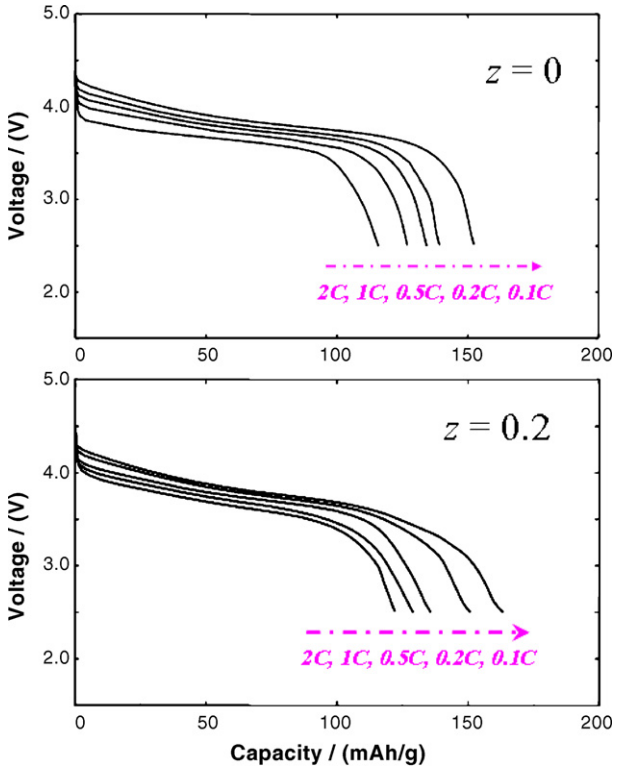

Fig. 15. The discharge curves of the sample with $z = 0$ and 0.2 at different discharge rates after cells were charged at a constant current density of 0.1C (20 mA g^{-1} and 0.2 mA cm^{-2}) in the voltage range of 4.5–2.5 V.

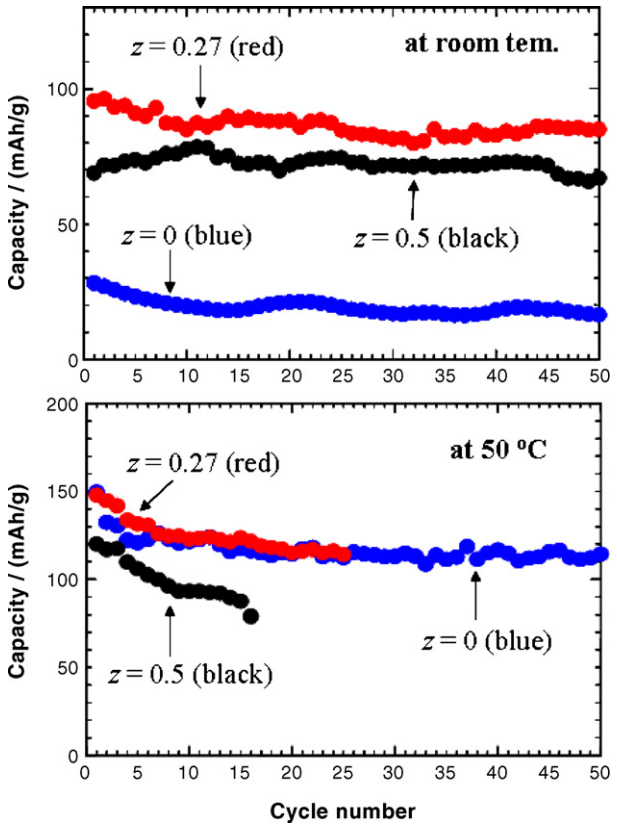

Fig. 16. Cycling performances of several typical samples in $Li_{1+z/3}Ni_{1/2-z/2}Ti_{1/2+z/6}O_2$ ($0 \le z \le 0.5$) cycled under the conditions executed in Figs. 8 and 9.

4. Conclusion

The triangle phase diagram of $LiNiO_2$–$LiTiO_2$–$Li[Li_{1/3}Ti_{2/3}]O_2$ is extremely similar to that of $LiNiO_2$–$LiMnO_2$–$Li[Li_{1/3}Mn_{2/3}]O_2$, except for structural difference of layered ordering. New Li–Ni–Ti–O series with the nominal composition of $Li_{1+z/3}Ni_{1/2-z/2}Ti_{1/2+z/6}O_2$ ($0 \le z \le 0.5$) in the phase diagram of $LiNiO_2$–$LiTiO_2$–$Li[Li_{1/3}Ti_{2/3}]O_2$, similar to the reported $Li[Li_{z/3}Ni_{1/2-z/2}Mn_{1/2+z/6}]O_2$ series in the phase diagram of $LiNiO_2$–$LiMnO_2$–$Li[Li_{1/3}Mn_{2/3}]O_2$, were prepared via homogeneous precursors derived from a spray-drying method. All samples could be identified as a pure phase with cubic rocksalt structure, in which Li^+, Ni^{2+} and Ti^{4+} evenly occupy the octahedral sites in cubic closely packed lattice of oxygen ions. They can be considered as the solid solution between cubic $LiNi_{1/2}Ti_{1/2}O_2$ and $Li[Li_{1/3}Ti_{2/3}]O_2$ (high temperature form). Some Li–Ni–Ti–O compounds displayed considerable capacities at room temperature and excellent electrochemical properties within respect to capacity, cycleability and rate capability at an elevated temperature of 50 °C. The optimized composition possibly lay in $0.2 \le z \le 0.27$, giving discharge capacities of >80 mAh g^{-1} at room temperature and >150 mAh g^{-1} at 50 °C at a constant current density of 20 mA g^{-1} in the voltage range of 4.5–2.5 V. These suggest that the disordered cubic structure in some cases can work as a good host structure for intercalation/deintercalation of Li^+. This can be possibly ascribed to nanosize effect of powder and 'pillar effect' of the framework consisting of Ti^{4+}. Electrochemical comparison of these compounds with $Li_{6/5}Ni_{2/5}Ti_{2/5}O_2$ indicated that the redox species of Ni^{4+}/Ni^{3+} and Ni^{3+}/Ni^{2+} should be responsible for the discharge capacity at the voltage of >3.0 V in $Li_{1+z/3}Ni_{1/2-z/2}Ti_{1/2+z/6}O_2$ ($0 \le z \le 0.5$), but it is Ni^{4+}/Ni^{3+} accounting for discharge capacity in $Li_{6/5}Ni_{2/5}Ti_{2/5}O_2$. Reduction of Ti^{4+} at a plateau of around 2.3 V could be clearly identified in $Li_{1+z/3}Ni_{1/2-z/2}LiTi_{1/2+z/6}O_2$ ($0.27 \le z \le 0.5$) at 50 °C after a deep charge associated with simultaneous expulsion of O and Li from structure during initial cycle. These findings may provide much valuable information to better understand electrochemical reaction mechanism in the related compounds and further design new electrode materials.

References

[1] T. Ohzuku, Y. Makimura, Chem. Lett. 8 (2001) 744.
[2] Y. Makimura, T. Ohzuku, J. Power Sources 119–121 (2003) 156.
[3] Z. Lu, D.D. Macneil, J.R. Dahn, Electrochem. Solid-State Lett. 4 (2001) A191.
[4] Z. Lu, J.R. Dahn, J. Electrochem. Soc. 149 (2002) A815.
[5] J.S. Kim, C.S. Johnson, J.T. Vaughey, M.M. Thackeray, S.A. Hackney, W. Yoon, C.P. Gray, Chem. Mater. 16 (2004) 1996.
[6] M.M. Thackeray, S.H. Kang, C.S. Johnson, J.T. Vaughey, S.A. Hachney, Electrochem. Commun. 8 (2006) 1531.
[7] K. Park, M.H. Cho, S.J. Jin, C.H. Song, K.S. Nahm, J. Power Sources 146 (2005) 281.
[8] J.H. Kim, Y.K. Sun, J. Power Sources 119–121 (2003) 166.
[9] Y. Arachi, H. Kobayashi, S. Emura, Y. Nakata, M. Tanaka, T. Asai, Chem. Lett. 32 (2003) 60.
[10] J. Reed, G. Ceder, Electrochem. Solid State Lett. 5 (2002) A145.
[11] W.S. Yoon, Y. Park, X. Yang, M. Balasubramanian, J. McBreen, C.P. Grey, Electrochem. Solid State Lett. 5 (2002) A263.
[12] J.S. Kim, C.S. Johnson, M.M. Thackeray, Electrochem. Commun. 4 (2002) 205.
[13] Y. Koyama, Y. Makimura, I. Tanaka, H. Adachi, T. Ohzuku, J. Electrochem. Soc. 151 (2004) 1499.
[14] L. Zhang, H. Noguchi, M. Yoshio, J. Power Sources 110 (2002) 57.
[15] H. Kobayashi, H. Sakaebe, H. Kageyama, K. Tatsumi, Y. Arachi, T. Kamiyama, J. Mater. Chem. 13 (2003) 590.
[16] L. Zhang, D. Li, X. Wang, H. Noguchi, M. Yoshio, Mater. Lett. 59 (2005) 2693.
[17] S.T. Myung, S. Komaba, N. Kumagai, Solid State Ion. 170 (2004) 139.
[18] E. Rossen, C.D.W. Jones, J.R. Dahn, Solid State Ion. 57 (1992) 311.
[19] C.H. Lei, J. Bareno, J.G. Wen, I. Petrov, S.H. Kang, D.P. Abraham, J. Power Sources 178 (2008) 422.
[20] H.H. Li, N. Yabuuchi, Y.S. Meng, S. Kumar, J. Breger, C.P. Grey, Y. Shao-Horn, Chem. Mater. 19 (2007) 2551.
[21] M.M. Thackeray, S.H. Kang, C.S. Johnson, J.T. Vaughey, R. Benedek, S.A. Hackney, J. Mater. Chem. 17 (2007) 3112.
[22] A.D. Robertson, P.G. Bruce, Electrochem. Solid-State Lett. 7 (2004) A298.
[23] A.R. Armstrong, P. Holzapfel, P. Novak, C.S. Johnson, S.H. Kang, M.M. Thackeray, P.G. Bruce, J. Am. Chem. Soc. 128 (2006) 8694.
[24] M. Castellanos, A.R. West, J. Mater. Sci. 14 (1979) 450.
[25] J. Kim, K. Amine, Electrochem. Commun. 3 (2002) 52.
[26] L. Zhang, X. Wang, H. Noguchi, M. Yoshio, K. Takada, T. Sasaki, Electrochim. Acta 49 (2004) 3305.
[27] H. Arai, S. Okada, Y. Sakurai, J. Yamaki, J. Electrochem. Soc. 144 (1997) 3177.
[28] S.H. Chang, S.G. Kang, S.W. Song, J.B. Yoon, J.H. Choy, Solid State Ion. 86–88 (1996) 171.
[29] L. Croguennec, E. Suard, P. Willmann, C. Delmas, Chem. Mater. 14 (2002) 2149.
[30] J.W. Joeng, S.G. Kang, J. Power Sources 123 (2003) 75.
[31] S.R.S. Prabaharan, M.S. Michael, H. Ikuta, Y. Uchimoto, M. Wakihara, Solid State Ion. 172 (2004) 39.
[32] Y. Sun, Z. Wang, X. Huang, L. Chen, J. Power Sources 146 (2005) 678.
[33] J.C. Anderson, M. Schieber, J. Phys. Chem. Solid 25 (1964) 961.
[34] J.C. Mikkelsen, J. Am. Ceram. Soc. 63 (1980) 331.
[35] H. Shigemura, M. Tabuchi, H. Sakaebe, H. Kobayashi, H. Kageyama, J. Electrochem. Soc. 150 (2003) A638.
[36] R.D. Shannon, Acta Crystallogr. A 32 (1976) 751.
[37] J.R. Dahn, U.V. Sacken, C.A. Michal, Solid State Ion. 44 (1990) 87.
[38] C.S. Johnson, J.S. Kim, A.J. Kropf, A.J. Kahaian, J.T. Vaughey, L.M.L. Fransson, K. Edstrom, M.M. Thackeray, Chem. Mater. 15 (2003) 2313.